ELSEVIER

Heterogeneous animal group models and their group-level alignment dynamics: An equation-free approach

Sung Joon Moon[a], B. Nabet[b], Naomi E. Leonard[b], Simon A. Levin[c], I.G. Kevrekidis[a],*

[a]Department of Chemical Engineering & Program in Applied and Computational Mathematics (PACM), USA
[b]Department of Mechanical and Aerospace Engineering, USA
[c]Department of Ecology and Evolutionary Biology, Princeton University, Princeton, NJ 08544, USA

Abstract

We study coarse-grained (group-level) alignment dynamics of individual-based animal group models for *heterogeneous* populations consisting of informed (on preferred directions) and uninformed individuals. The orientation of each individual is characterized by an angle, whose dynamics are nonlinearly coupled with those of all the other individuals, with an explicit dependence on the difference between the individual's orientation and the instantaneous average direction. Choosing convenient coarse-grained variables (suggested by uncertainty quantification methods) that account for rapidly developing correlations during initial transients, we perform efficient computations of coarse-grained steady states and their bifurcation analysis. We circumvent the derivation of coarse-grained governing equations, following an equation-free computational approach.
© 2006 Elsevier Ltd. All rights reserved.

1. Introduction

Coordinated motions and pattern formation have been studied for a wide range of biological organisms, from bacteria and amoebae to fish, from birds and wildebeest to humans (Ben-Jacob et al., 2000; Camazine et al. (2001); Parrish et al., 2002; Partridge, 1982; Weidlich, 1991; Wilson, 1975). Animal groups often behave as if they have a single mind, displaying remarkable self-organized behavior. At one extreme, the individuals seem to need little information transfer (e.g., fish schools), while at the other end the information exchange occurs in highly integrated ways through long-term associations among the individuals (e.g., honeybee hives and human communities). Controlling such an organized behavior in groups of artificial objects, including autonomous underwater vehicles (Leonard et al., 2007) and groups of autonomous agents (Jadbabaie et al., 2003), has received extensive attention in contemporary control theory. Challenges in both natural and engineering settings involve understanding which patterns emerge from the interaction among individual agents.

Selected laboratory experiments have shed some light on the schooling mechanism (Hunter, 1966; van Olst and Hunter, 1970; Partridge and Pitcher, 1979, 1980; Pitcher et al., 1976). It still remains unclear, however, how the individual-level behavior and group-level ("macroscopic", or coarse-grained) patterns are related. More precise experiments using three-dimensional tracking of every individual in a population should lead to better understanding of this linkage. An ultimate experimental study with precise control of every relevant detail may not be possible, yet appropriate mathematical models would provide a venue to establish behavioral cause, as one can consider different hypothetical individual-level interaction rules selectively (see e.g., Flierl et al., 1999).

Several different individual-based models have been proposed, which reproduce certain types of collective behavior in animal groups (e.g., see Aoki, 1982; Reynolds, 1987; Deneubourg and Goss, 1989). Self-organization emerges also in a wide spectrum of physical and chemical

*Corresponding author. Tel.: +1 609 258 2818; fax: +1 609 258 0211.
E-mail address: yannis@princeton.edu (I.G. Kevrekidis).

systems, some of which (e.g., crystals and ferromagnetic materials) exhibit apparent similarities with emergent patterns observed in animal groups. Vicsek et al. (1995) have introduced a discrete-time model of self-driven particles, or self-propelled particles (SPP), based on near-neighbor rules that are similar with those in the ferromagnetic XY model (Kosterlitz and Thouless, 1973). The authors analyzed statistical properties of the model, including phase transition and scaling (Vicsek et al., 1995). A long-range interaction has been incorporated into the SPP model (Mikhailov and Zanette, 1999), and continuum, "hydrodynamic" versions of this model have been introduced (Toner and Tu, 1995, 1998; Topaz et al., 2006). Recently, Couzin et al. (2002, 2005) have introduced a model to provide insights into the mechanism of decision making in biological systems, which reproduces many important observations made in the field, and provides new insights into these phenomena. A review for various models can be found in Parrish et al. (2002) and Czirók and Vicsek (2001).

The models of Couzin et al. (2005), and most other such models, incorporate various detailed mechanistic steps. These shed light on the role of leadership and imitation, and produce a number of surprising results, such as the influence that a few "informed" individuals can have on large collectives. What is needed now are efforts to simplify those models, and to show especially what properties of the microscopic simulators are essential to explain that behavior. For some models, closure schemes are available (Flierl et al., 1999); but more generally, though we may suspect that closures exist, we cannot derive explicit expressions for them. In such circumstances, we need methods such as those used in this paper; we perform the coarse-grained dynamical analysis by circumventing the derivation of governing equations, using an equation-free computational approach (Theodoropoulos et al., 2000; Kevrekidis et al., 2003). A particular goal is to understand how much of the specific spatial detail is fundamental to the behavior. But turning to the Kuramoto-type approximation, where the interaction is assumed to be global, we deliberately ignore local effects. To the extent that the models fail to explain observed types of behavior, we will need to turn next to more detailed models.

Most of previously proposed models concern populations of *homogeneous* (or indistinguishable) individuals. Furthermore, the dynamical analysis in the literature is often limited to a small subset of the entire parameter space, and a systematic classification of possible global dynamics remains elusive. In the current paper, we study the *coarse-grained* alignment dynamics of individual-based animal group models. The measurement of the mean angular deviation of fish schools (e.g., clupeids and scombroids; see Atz, 1953; Hunter, 1966) showed that it varies continuously from no alignment to practically perfect alignment. We account for this continuous change by heterogeneity ("quenched noise"; characterized by parameters of random variables drawn from a prescribed

distribution function) and the coupling strength. Our approach is flexible in that the heterogeneity can be introduced in various places in the model, and the way we analyze different heterogeneity cases does not require any significant modification.

The rest of the paper is organized as follows: models for homogeneous and heterogeneous animal groups are described in Sections 2.1 and 2.2, and our approach, equation-free polynomial chaos, is explained in Sections 2.3 and 2.4. Coarse-grained dynamical analysis and its comparison with fine-scale dynamics, for a system of two informed individuals and a large number of heterogeneous uninformed individuals, are presented in Section 3. The case of two groups of heterogeneous informed individuals is presented in Section 4. We conclude with a brief discussion in Section 5.

2. Models and methods

2.1. A "minimal" model for identical individuals

We briefly discuss a "minimal" model proposed by Nabet et al. (2006), which we extend in our study. It concerns the alignment dynamics of a homogeneous population of *indistinguishable* N individuals with two subgroups of informed individuals ("leaders") with populations N_1 and N_2, respectively, and N_3 uninformed individuals ("followers"), where $N = N_1 + N_2 + N_3$:

$$\frac{d\psi_1}{dt} = \sin(\Theta_1 - \psi_1) + \frac{K}{N}N_2\sin(\psi_2 - \psi_1)$$
$$+ \frac{K}{N}N_3\sin(\psi_3 - \psi_1),$$

$$\frac{d\psi_2}{dt} = \sin(\Theta_2 - \psi_2) + \frac{K}{N}N_1\sin(\psi_1 - \psi_2)$$
$$+ \frac{K}{N}N_3\sin(\psi_3 - \psi_2),$$

$$\frac{d\psi_3}{dt} = \frac{K}{N}N_1\sin(\psi_1 - \psi_3) + \frac{K}{N}N_2\sin(\psi_2 - \psi_3). \quad (1)$$

Here ψ_k characterizes the average direction of the individuals in each of the two informed subgroups for $k = 1, 2$ and the average direction of the uninformed individuals for $k = 3$. Θ_k is the corresponding informed, preferred direction (Θ_1 can be set to zero without loss of generality) and $K(\geqslant 0)$ is the coupling strength. This minimal model corresponds to the reduced system of the following system of N individuals (Nabet et al., 2006):

$$\frac{d\theta_j}{dt} = \sin(\Theta_1 - \theta_j) + \frac{K}{N}\sum_{l=1}^{N}\sin(\theta_l - \theta_j) \quad \text{for } 1\leqslant j\leqslant N_1,$$

$$\frac{d\theta_j}{dt} = \sin(\Theta_2 - \theta_j) + \frac{K}{N}\sum_{l=1}^{N}\sin(\theta_l - \theta_j)$$
$$\text{for } N_1 + 1 \leqslant j \leqslant N_1 + N_2,$$

$$\frac{d\theta_j}{dt} = \frac{K}{N}\sum_{l=1}^{N}\sin(\theta_l - \theta_j) \quad \text{for } N_1 + N_2 + 1\leqslant j\leqslant N, \quad (2)$$

where the angle θ_j characterizes the direction in which the jth individual is heading (we will refer to it as "orientation"). The average direction ψ_k is defined as the angle of the average of the phasors (when each individual's dynamical state is considered as a phasor of unit radius and a phase angle) of the individuals in the kth subgroup; ρ_k is the magnitude of the average of the phasors. Formally, this is written as

$$\rho_1 e^{i\psi_1} \equiv \frac{1}{N_1} \sum_{j=1}^{N_1} e^{i\theta_j},$$

$$\rho_2 e^{i\psi_2} \equiv \frac{1}{N_2} \sum_{j=N_1+1}^{N_1+N_2} e^{i\theta_j},$$

$$\rho_3 e^{i\psi_3} \equiv \frac{1}{N_3} \sum_{j=N_1+N_2+1}^{N} e^{i\theta_j}.$$

The large population model in Eq. (2) has a separation of time scales. Individuals within each subgroup synchronize quickly, i.e., ρ_k quickly converges to 1. The slow dynamics are described by the reduced system (Eq. (1)) where the variables ψ_k characterize the *lumped behavior* of each of the three subgroups.

It is assumed that the alignment (orientational) dynamics are independent of the translational counterpart (Sepulchre et al., 2005); hence, the dynamical state of an individual can be characterized by its orientation. The functional form for mutual interaction is borrowed from the well-known Kuramoto model (Kuramoto, 1984), a prototypical model for coupled nonlinear oscillators. This simplified global interaction model is consistent with an observation that the strongest correlations are observed between the (speed and) direction of the individual and the average (speed and) direction of the entire school (Partridge, 1982): in the mean-field form of the Kuramoto model, the interaction term can be rewritten as

$$\frac{1}{N} \sum_{l=1}^{N} \sin(\theta_l - \theta_j) = r \sin(\psi - \theta_j), \quad \text{where } r e^{i\psi} \equiv \frac{1}{N} \sum_{l=1}^{N} e^{i\theta_l}.$$
$$(3)$$

In this alternate expression, the dependence on the difference between the individual direction and the average direction stands out explicitly. In the absence of coupling ($K = 0$), each leader eventually heads for its preferred direction. Nontrivial dynamical behavior for the minimal model (Eq. (1)) is studied in Nabet et al. (2006); bifurcations are analyzed for the global phase space in the case $N_1 = N_2$ and $N_3 = 0$.

2.2. Extension to heterogeneous populations

The aforementioned models concern populations of *homogeneous* subgroups, where the individuals in each subgroup quickly synchronize, nearly perfectly ($\rho_k \sim 1$), during the initial transients (Nabet et al., 2006). In the more general case, the mean angular deviation of fish schools is

finite (Atz, 1953; Hunter, 1966), which is not captured in this "minimal" model. We extend the model to account for the distribution of directions within schools, assuming it arises from the *heterogeneity* among the group members. We introduce the heterogeneity in the following two ways:

(I) *Two leaders and many heterogeneous followers*—Firstly, we consider the cases when the population consists of two leaders (which possibly represent lumped behavior of groups of homogeneous leaders) and $N (\gg 1)$ followers:

$$\frac{d\psi_1}{dt} = \sin(\Theta_1 - \psi_1)$$
$$+ \frac{K}{N+2} \left[\sum_{j=1}^{2} \sin(\psi_j - \psi_1) + \sum_{j=1}^{N} \sin(\theta_j - \psi_1) \right],$$

$$\frac{d\psi_2}{dt} = \sin(\Theta_2 - \psi_2)$$
$$+ \frac{K}{N+2} \left[\sum_{j=1}^{2} \sin(\psi_j - \psi_2) + \sum_{j=1}^{N} \sin(\theta_j - \psi_2) \right],$$

$$\frac{d\theta_i}{dt} = \omega_i + \frac{K}{N+2} \left[\sum_{j=1}^{2} \sin(\psi_j - \theta_i) + \sum_{j=1}^{N} \sin(\theta_j - \theta_i) \right]$$
for $1 \leqslant i \leqslant N$, 					(4)

where the heterogeneity is accounted for through the tendency to deviate from the average direction, characterized by ω_i, an i.i.d. random variable drawn from a prescribed distribution function $g(\omega)$ (of standard deviation σ_ω with mean value zero). For notational convenience, we drop the subscript of a random variable to represent a vector variable of the appropriate length (cf. ω_i and ω). As Θ_1 can be set to zero without loss of generality, Θ_2 and K are control parameters. In the current study, we consider $g(\omega)$ to be Gaussian, but our analysis is not limited to this particular choice.

(II) *Two groups of heterogeneous leaders*—Secondly, we consider two groups of heterogeneous leaders without any followers, focusing only on the dynamics among leaders. The heterogeneity is accounted for by introducing randomness in the angles preferred by the leaders. The orientations of the leaders in each group are denoted by χ_i's and ϕ_i's (of sizes N_1 and N_2), respectively:

$$\frac{d\chi_i}{dt} = \sin(\mathscr{X}_i - \chi_i) + \frac{K}{N_1+N_2} \left[\sum_{j=1}^{N_1} \sin(\chi_j - \chi_i) \right.$$
$$\left. + \sum_{j=1}^{N_2} \sin(\phi_j - \chi_i) \right] \quad \text{for } 1 \leqslant i \leqslant N_1,$$

$$\frac{d\phi_i}{dt} = \sin(\Phi_i - \phi_i) + \frac{K}{N_1+N_2} \left[\sum_{j=1}^{N_1} \sin(\chi_j - \phi_i) \right.$$
$$\left. + \sum_{j=1}^{N_2} \sin(\phi_j - \phi_i) \right] \quad \text{for } 1 \leqslant i \leqslant N_2,$$
					(5)

where the preferred angles $\mathscr{X}_i$ and Φ_i are randomly drawn from prescribed distributions $g_1(\mathscr{X})$ and $g_2(\Phi)$ (i.e., i.i.d. random variables of standard deviations $\sigma_{\mathscr{X}}$ and σ_Φ),

respectively. We set $\langle \mathcal{X} \rangle = 0$, and will vary $K (\geqslant 0)$ and $\langle \Phi \rangle$ ($\in [0, \pi]$) as control parameters (and investigate some cases of different values of $\sigma_{\mathcal{X}}$ and σ_{Φ} in Section 4.2).

2.3. Wiener polynomial chaos

The Kuramoto model, a paradigm for all-to-all, phase-coupled oscillator models, has been extensively studied and used to shed light on many synchronization phenomena (Kuramoto, 1984; Acebrón et al., 2005, and references therein). This model has the property that, in the full synchronization regime (of large enough K values), phase angles become quickly correlated with (or "sorted" according to) the natural frequencies during the initial short transients (Moon et al., 2006). Similar correlations (between the angles and heterogeneity random variables) are expected to arise in the current model (which is indeed the case, as will be shown later in Fig. 1), since the coupling term is qualitatively similar. As in Moon et al. (2006), we choose expansion coefficients in Wiener polynomial chaos as coarse-grained "observables", to explore low-dimensional, coarse-grained dynamics.

Wiener(-Hermite) polynomial chaos was introduced by Wiener (1938), who represented a random process in terms of functional expansions of Wiener process (historically, this method has been termed as polynomial "chaos", because of its initial usage on homogeneous chaos, such as turbulence and Brownian motion, rather than the nature of the method). Ghanem and Spanos (1991) later extended this idea to treat random processes as functional expansions of random variables, or elements in the Hilbert space of random functions, in which a spectral representation in terms of polynomial chaos is identified. The projections (or coefficients) on the polynomial base then can be determined through a Galerkin approach. This method was subsequently applied in uncertainty quantification of various problems (e.g., see Ghanem, 1999; Jardak et al., 2002), and has been extended to general situations using the Askey scheme (Xiu and Karniadakis, 2002; now known as generalized polynomial chaos).

In this method, dependent random variables (θ of the followers for the case (I), and χ and ϕ for the case (II)) are expanded in polynomials of independent random variables (ω, or $\mathcal{X}$ and Φ) using appropriately chosen basis functions. Details for the two cases are as follows:

(I) *Two leaders and many heterogeneous followers*—For convenience, we introduce the unit Gaussian random variable $\xi \equiv \omega / \sigma_{\omega}$. Using this newly defined variable, we
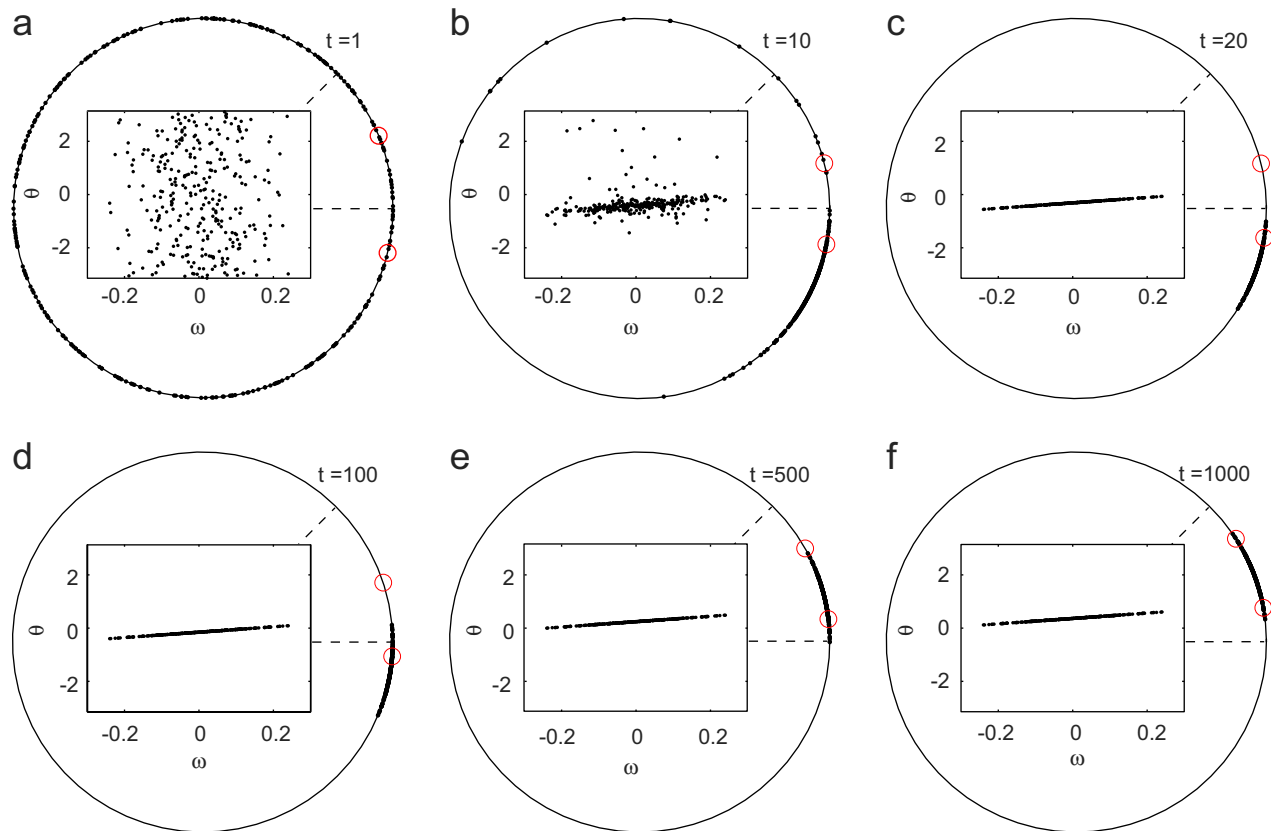

Fig. 1. Direct integration of a system of two leaders (open circles; dashed lines indicate preferred angles) and 300 followers (dots), initialized from uniformly distributed orientations with randomly assigned heterogeneity variable (i.e., no initial correlations between θ and ω), is shown for an initial transient ((a)–(c)), and for much longer time scales ((d)–(f)). Insets illustrate time evolution of the followers' orientations on the $\theta - \omega$ plane, where strong correlations develop during a short time $t \sim 10$. After that, the leaders and followers, the latter effectively as a "unit", slowly drift to the stable steady state. It takes of the order of $t \sim 10^3$ for the system to asymptotically converges to this final state ($K = 1.0$; $\Theta_2 = \pi/4$). When correlations fully develop, after initial transients, we functionally expand θ in terms of ω and use the expansion coefficients as our coarse-grained variables.

expand $\theta(\omega, t)$ (i.e., $\theta(\xi, t)$) in Hermite polynomials of ξ [$H_0(\xi) = 1$, $H_1(\xi) = \xi$, $H_2(\xi) = \xi^2 - 1$, $H_3(\xi) = \xi^3 - 3\xi, \ldots$]:

$$\theta(\xi, t) = \sum_{n=0}^{p} \alpha_n(t) H_n(\xi), \tag{6}$$

where p is the highest order retained in the truncated series, H_n is the nth Hermite polynomial, and the α_n's are the expansion coefficients which will be referred to simply as "chaos coefficients" in this paper. Wiener polynomial chaos, utilizing Hermite polynomials as basis functions, is the appropriate choice for Gaussian random variables that we consider in the present study. The probability density function of the Gaussian random variables appears as the weighting function in the orthogonality relations of Hermite polynomials, and the Hermite polynomial expansion is suggested to converge exponentially for Gaussian processes (Lucor et al., 2001). For other random variables, use of different basis functions (for instance, Legendre polynomials for uniform random variables) has been suggested for fast convergence, which is the basis of the development of the generalized polynomial chaos (Xiu and Karniadakis, 2002).

We choose the first few nonvanishing chaos coefficients α_n's, as well as the orientations of the leaders (ψ_1 and ψ_2), to be the coarse-grained "observables". Due to symmetry, all the even order α_n's vanish, except for the zeroth order α_0 that corresponds to the average direction of the followers. Geometrically, α_1 and α_3, respectively, represent a measure for the linear order spread of the angles (the "slope" between θ and ω) and the cubic order measure. In the continuum limit ($N \to \infty$), the chaos coefficients can be exactly determined using the orthogonality relations for Hermite polynomials. However, in the *finite* cases of single realization we consider, $N \sim O(10^2)$, those relations hold only approximately, and the coefficients are evaluated using least squares fitting, following Moon et al. (2006).

(II) *Two groups of heterogeneous leaders*—In the second case, we expand χ and ϕ in terms of $\mathscr{X}$ and Φ, respectively:

$$\chi = \sum_{n=0}^{p} \alpha_n H_n(\zeta),$$

$$\phi = \sum_{n=0}^{p} \beta_n H_n(\eta), \tag{7}$$

where the chaos coefficients $\boldsymbol{\alpha}$ and $\boldsymbol{\beta}$ are the coarse "observables" of our choice, H_n's are Hermite polynomials (for Gaussian g_1 and g_2), and $\zeta \equiv \mathscr{X}/\sigma_\chi$ and $\eta \equiv \Phi/\sigma_\phi$ are unit Gaussian random variables.

2.4. "Equation-free" computational approach

A prerequisite to *coarse-grained* dynamical analysis (which is the main goal of the current study) is, in a traditional sense, an explicit derivation of coarse-grained governing equations. In principle, such equations for chaos coefficients, in the continuum limit ($N \to \infty$), might be obtained through a stochastic Galerkin method (Ghanem and Spanos, 1991).

In the present study, we do not even attempt to derive such equations. We circumvent their derivation by using an equation-free multiscale computational approach (Theodoropoulos et al., 2000; Kevrekidis et al., 2003, 2004). This approach enables us to explore the coarse-grained dynamics without the assumption of the continuum limit. The premise of this approach is that coarse-grained governing equations conceptually *exist*, but are not explicitly available in closed form. This approach is based on the recognition that short bursts of appropriately initialized microscopic (fine-scale) simulations during a time horizon ΔT and the projection of the results onto coarse-grained variables, say x, result in time steppers (mappings) for those variables $\boldsymbol{\Phi}_{\Delta T}$ (which is effectively the same as the discretization of unavailable equations):

$$x_{n+1} = \boldsymbol{\Phi}_{\Delta T}(x_n). \tag{8}$$

One then processes the results of the short simulations to estimate various coarse-grained quantities (such as time derivatives, action of Jacobians, residuals) to perform relevant coarse-grained level numerical computations, as if those quantities were obtained from coarse-grained governing equations. For instance, one can *integrate* unavailable governing equations in time (coarse projective integration; see below), or compute the steady states of the above coarse time stepper, by utilizing fixed point algorithms (such as Newton–Raphson or Newton–GMRES).

Equation-free computations consist of the following steps:

1. Identify coarse-grained variables ("coarse observables") that sufficiently describe both the micro- and macroscopic dynamics; in our study, they are α_n's (and β_n's). For convenience, we denote the microscopic (macroscopic) descriptions by θ ($\boldsymbol{\alpha}$).
2. Choose an appropriate *lifting* operator μ_L, which maps $\boldsymbol{\alpha}$ to one (or more) consistent description(s) θ (for the purposes of variance reduction and ensemble averaging). In the current study, this can be achieved by using the relations in Eqs. (6) and (7); once random variables are drawn, these relations are used to obtain corresponding θ.
3. Starting from lifted initial condition(s) $\theta(t_0) = \mu_L(\boldsymbol{\alpha}(t_0))$, run the microscopic simulator to obtain $\theta(t_0 + \Delta T)$ at a later time ($\Delta T \geqslant 0$).
4. Use an appropriate *restriction* operator $\mathscr{M}_R$ (least squares fitting, in the current study) which maps the microscopic state(s) to the macroscopic description $\boldsymbol{\alpha}(t_0 + \Delta T) = \mathscr{M}_R(\theta(t_0 + \Delta T))$, which effectively results in time series of coarse observables, or their coarse time stepper $\boldsymbol{\Phi}_{\Delta T}$; $\boldsymbol{\alpha}(t_0 + \Delta T) \equiv \boldsymbol{\Phi}_{\Delta T}(\boldsymbol{\alpha}(t_0))$.

5. Apply desired numerical techniques using the coarse-grained variables obtained from step 4 and repeat some of the above steps as needed.

An extensive discussion can be found in Kevrekidis et al. (2003, 2004).

3. Results for case I

Direct integration of the "fine-scale" model of Eq. (4) in the strong coupling regime ($K = 1.0$, $\sigma_\omega = 0.1$), started from randomly assigned orientations and the heterogeneity variable (the latter is a Gaussian random variable), illustrates that a strong correlation between θ and ω develops during a short, initial transient time; the orientations of the followers quickly become a monotonically increasing function of their heterogeneity variable (Fig. 1), after which they slowly drift as a "unit" until they settle down in the final steady state. During the latter slow drift, the system can be described as two leaders and a *single* "clump" of followers, whose coarse-grained states can be successfully described by a small number of chaos coefficients. A similar time scale separation exists in the model of homogeneous populations. In this case, followers quickly collapse asymptotically to the *same* direction (Nabet et al., 2006).

3.1. Computations of steady states

We begin by accelerating the approach to a stable steady state using an equation-free algorithm, the coarse projective integration method (Gear and Kevrekidis, 2003). In contrast to a conventional, direct integration of the full fine-scale model during the *entire* time (until sufficient convergence to stable, final states), this method exploits smoothness in the coarse variables (estimated through a direct integration during a *short* time), in order to extrapolate and take a large projective time step (compared to the original integration time-step size). This saves computational effort. The procedure consists of (i) *lifting* (appropriate initialization of the fine-scale simulator, an integrator of Eq. (4), consistent with prescribed coarse-grained values), (ii) *direct integration* of the microscopic simulator during a relatively short time interval (but long enough to accurately estimate local coarse-grained time derivatives), (iii) *restriction* (of fine-scale description onto coarse-grained variables), and (iv) *taking a projective step* (using a traditional numerical integration scheme such as forward Euler). The computational payoff of this method depends on the ratio between a short direct integration time interval, the projective time-step size, and the computational effort required for lifting/restriction procedures (see e.g., Rico-Martinez et al., 2004). More importantly, successful computation of steady states through this method naturally attests to the *validity* of the chosen coarse-grained observables in describing *both* fine-scale and coarse-grained states.

Projective integration using five coarse-grained variables (ψ_1, ψ_2, and the first three nonvanishing α_n's; α_0, α_1, and α_3) follows virtually the same trajectories of the full, direct integration (Fig. 2), even if ω is *newly* drawn at each lifting; the agreement is even better if the same ω were used (hence the dynamics are fully deterministic). Both *lifting* (simply using Eq. (6)) and *restriction* (least squares fitting) operations require minimal computational efforts. Therefore, the computational efficiency in the present case is
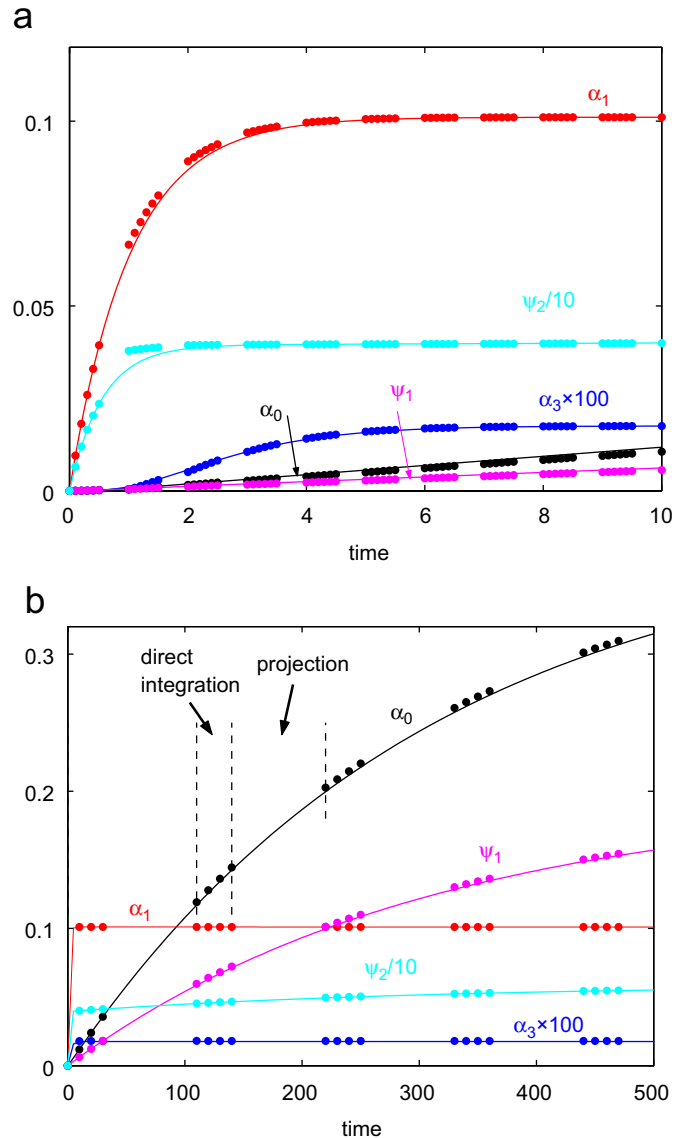
Fig. 2. (Color online) Accelerated computation of stable steady states via coarse projective integration using five coarse-grained variables, shown here for two different time scales ($K = 1.0$; $\Theta_2 = \pi/4$). Initially, all the values are assigned to be 0. Both α_1 and α_3 reach their steady state values relatively quickly (see (a)), while the others are slowly varying (see (b); they are still varying at $t = 500$). Dots represent the time intervals during which short direct integration is performed (and restricted), in the course of the projective integration using forward Euler method. Solid lines represent the trajectories of direct full integration during the entire time. Higher efficiency can be achieved by optimally choosing the time horizon for the direct integration, the projection stepsize, and projection method.

Table 1
A coarse steady state computation at $K = 1.0$ and $\Theta_2 = \pi/4$ for $N = 300$, using the Newton–GMRES method. Values at each iteration have been averaged over an ensemble of 100 realizations. The last column shows relative residuals

Iteration	ψ_1	ψ_2	α_0	α_1	α_3	Residuals
0	0.0	0.0	0.0	0.0	0.0	1.0
1	3.421×10^{-5}	4.143×10^{-1}	3.478×10^{-5}	5.963×10^{-2}	2.969×10^{-9}	2.680×10^{-3}
2	8.871×10^{-4}	3.900×10^{-1}	9.293×10^{-4}	8.632×10^{-2}	2.435×10^{-5}	8.135×10^{-4}
3	1.245×10^{-3}	3.969×10^{-1}	1.991×10^{-3}	9.819×10^{-2}	9.387×10^{-5}	2.056×10^{-4}
4	1.338×10^{-1}	5.275×10^{-1}	2.679×10^{-1}	1.010×10^{-1}	8.338×10^{-4}	3.820×10^{-5}
5	1.959×10^{-1}	5.896×10^{-1}	3.929×10^{-1}	1.010×10^{-1}	1.754×10^{-4}	3.660×10^{-7}
6	1.958×10^{-1}	5.896×10^{-1}	3.927×10^{-1}	1.010×10^{-1}	1.760×10^{-4}	6.513×10^{-12}

nearly exclusively determined by the projective step size, which is a factor of about four in Fig. 2; with a more sophisticated projection algorithm, a higher efficiency can be obtained. We see that both α_1 and α_3 reach their steady state values quickly ($t \sim 5$), showing that the correlation between θ and ω are fully developed by then. However, the other chaos coefficient α_0 (representing the average direction) slowly drifts toward the steady state, and so do ψ_1 and ψ_2 (note that it is still varying at $t = 500$); the computation of an asymptotic, steady state requires a very long time integration.

Direct integration (including projective integration) cannot compute unstable steady states and are inappropriate for stability computations and parametric bifurcation studies. Both stable and *unstable* steady state values can be systematically (and much more efficiently than the projective integrations) computed by applying coarse-grained fixed point algorithms to the steady state condition of Eq. (8), i.e., $\mathbf{x} - \mathbf{\Phi}_{\Delta T}(\mathbf{x}) = 0$, in *much lower* dimension than that of individual level. We use the coarse Newton–GMRES (Kelley, 1995), a matrix-free, method to compute coarse-grained fixed points. We observe that the algorithm accurately converges within a few steps (Table 1); the converged values are accurately consistent with the restricted values of the fixed point solution of the detailed (i.e., $(N + 2)$-dimensional) problem, within prescribed convergence tolerance. By combining a coarse fixed point algorithm with pseudo-arc-length continuation (Keller, 1987), we numerically compute coarse-grained bifurcation diagrams in the following sections. The computational efficiency of the coarse fixed point algorithm varies with the choice of the initial guess for the iteration. With a totally uneducated guess, it could take even longer than the direct integration (note that the latter never computes the exact solutions); however, during the continuation computation shown below, a good initial guess is always available from the previous parameter value(s), and even several orders of magnitude of computational efficiency can be achieved.

3.2. Types of fine-scale dynamical behavior

We first analyze the detailed $(N + 2)$-dimensional fine-scale model in the full synchronization regime, in order to obtain insights on fine-scale dynamics to be compared with our coarse-grained analysis below. We use AUTO2000 (Doedel et al., 2000) to compute the fine-scale bifurcation diagrams as functions of Θ_2 at a fixed value of K; only projections for one leader (ψ_2) are shown in Fig. 3 and for one follower in Fig. 4(a). All the other followers exhibit essentially the same dynamical behavior as the one shown here (except for some quantitative differences).

The interaction between the individuals causes the steady state directions of the leaders to deviate from the preferred angles 0 and Θ_2, respectively. Such deviation can occur in two directions, either toward the region bounded by $[0, \Theta_2]$ (an "obvious" steady state where followers are directed in between the directions of the leaders; see Fig. 3(b)) or the other way around (e.g., Fig. 3(a)). The analysis shows that for small Θ_2 values only the former state is stable, while for large values, both of these states become stable. The branches for "obvious" stable steady states, which correspond to lower straight solid lines, exhibit no bifurcations (see Figs. 3 and 4(a)). On the other branches, forward pitchfork bifurcations at some critical value of Θ_2 give birth to another stable branch (a state on this stable branch is shown in Fig. 3(a)), as well as two unstable asymmetric solution branches, hence the population becomes bistable. The critical value of Θ_2 for the onset of the bistability depends on K (precisely speaking, K/σ_ω); the critical value is $\Theta_2 \sim 0.45(2.2)$ at $K = 1.0(0.5)$. As K decreases further, the critical value monotonically increases until fully synchronized steady states lose stability at some critical value of K.

3.3. Coarse-grained dynamics

We now compute coarse-grained steady state solutions. A coarse-grained bifurcation diagram for α_0 (representing the average direction of the followers) is compared with the corresponding diagram observed for *one* follower, in Figs. 4(b) and (a); (b) is a blowup of the region around the bifurcation. Both sides of the bifurcation point can be described by the *same* set of coarse-grained observables, which clearly summarize group level dynamical behavior of the followers before and after the bifurcation.
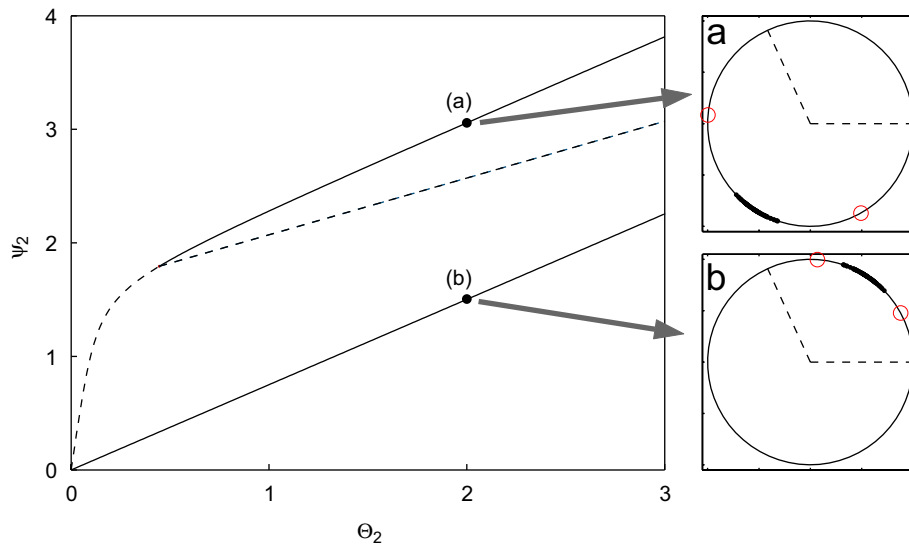
Fig. 3. (Left panel) A bifurcation diagram observed on one leader ψ_2, computed using AUTO2000 ($K = 1.0$). Solid (dashed) lines represent stable (unstable) branches. There exist a few other unstable branches that are not shown here. At some critical value of Θ_2, an unstable state in the upper branch undergoes a forward pitchfork bifurcation; two unstable states coincide. The lower branch of "trivial" solutions does not exhibit any bifurcation. (Right panels) Snapshots of two (symmetric) stable states in the bistable regime ($\Theta_2 = 2.0$), marked by dots in the left panel.

As K decreases in the Kuramoto model, oscillators get desynchronized (Kuramoto, 1984), starting with the oscillator with the maximum value of $|\omega_i|$ (the "extreme" oscillator) through a saddle-node (actually a "sniper") bifurcation on a limit cycle (Moon et al., 2006). We expect the same type of bifurcation to occur in this model. However, when we try to compute the coarse-grained steady states as functions of K using the previously mentioned five coarse variables via coarse Newton–GMRES method and pseudo-arc-length continuation, neither a bifurcation nor an unstable branch is appropriately identified. The computation, initialized at large K-steady states, accurately follows stable branches down to some critical value of K (where the transition occurs), and then fails to converge. Our coarse-grained observables are not sufficient to describe the states on the "other side" of the bifurcation point, as we will explain below.

A fine-scale bifurcation diagram (computed using AUTO2000) obtained by starting from a stable steady state on the lower branch in Fig. 3 is shown in Fig. 5(a). Here the diagrams for two leaders and only a few followers, including the extreme one, are shown. We find that both stable and unstable branches for each angle nearly coincide for all the individuals (see inset of Fig. 5(a)), except for the extreme one. As the difference between stable and unstable branches (at the same value of K) is appreciable *only* when observed on this extreme oscillator, a smooth mapping between θ and ω does not prevail for unstable states, and the previously used chaos coefficients are not appropriate any more.

Taking these observations into account, it is easy to remedy the situation as follows: the fact that stable and unstable branches nearly coincide, discounting the extreme follower, suggests that all the individuals *except for the extreme follower* can be again described by the same set of chaos coefficients. Thus, we treat the orientation of the extreme one separately (introducing it as an additional coarse-grained variable), and discount it from the polynomial chaos expansion. (From the fact that the extreme follower gets desynchronized at the transition, one can also intuitively see that followers have to be considered as a combination of a clump of synchronized "bulk" and a separate, extreme one.) We compute the solutions with continuation, using this new set of *six* coarse variables, which captures the bifurcation and appropriately describes the unstable steady states (Fig. 5(b)); we have analyzed exactly the same realization used in Fig. 5(a) for direct comparison. When bifurcation diagrams are computed for ensembles of many realizations, an uncertainty will arise in the exact quantification of the bifurcation point, due to the fluctuation of finite-dimensional random variables among realizations, while the results are qualitatively the same as those of a single realization (Xiu et al., 2005).

The coarse bifurcation results shown in Fig. 5(b) illustrate that the steady state directions of the leaders and the average direction of followers (α'_0, discounting the extreme one; a prime is added to distinguish it from the previously used notation) are virtually the same for a range of K. Only higher order chaos coefficients (only α'_1 is shown in Fig. 5) appreciably vary as a function of K, which means that individuals spread more widely as K decreases, until the extreme one eventually starts to oscillate freely, while the average steady state direction remains the same.
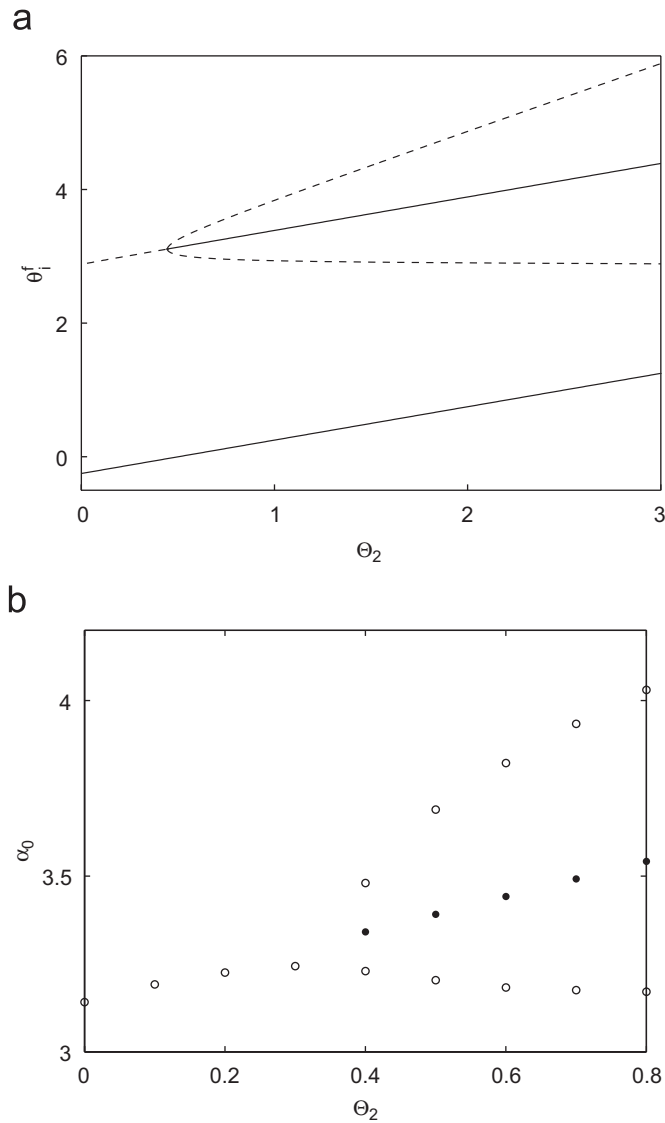
Fig. 4. (a) A bifurcation diagram observed on one (arbitrarily chosen) follower, as a function of Θ_2 ($K = 1.0$), computed using AUTO2000 (the same case as in Fig. 3). Superscript 'f' has been added to emphasize that this is the orientation of *a follower*. A few other existing unstable branches are not included here. The upper branch undergoes a pitchfork bifurcation and becomes stable. (b) A coarse bifurcation diagram observed on α_0 (average direction), obtained by the coarse Newton–GMRES method with pseudo-arc-length continuation. Only a blowup around the bifurcation point is shown. Coarse-grained dynamics exhibit the same structure as in the fine-scale level. Filled (open) circles represent stable (unstable) steady-states.

Fig. 5. (Color online) (a) A bifurcation diagram observed on a few followers, including the one with the maximum of $|\omega_i|$ (the "extreme" follower), as a function of K ($\Theta_2 = \pi/4$), computed using AUTO2000. A critical value where the extreme individual gets desynchronized corresponds to a saddle-node bifurcation point on a limit cycle (a "sniper" bifurcation). Except for the extreme follower, stable and unstable branches nearly coincide (see the inset). (b) In order to capture the fine-scale bifurcation, the angle of the extreme follower has to be discounted from the chaos expansion and considered as an *extra* coarse-grained variable (see text). We distinguish these chaos coefficients (from the ones used so far) by adding a prime. It was computed via the coarse Newton–GMRES method with continuation.

4. Results for case II

4.1. Dynamics of statistically similar groups

Here, we explore both the fine-scale and coarse-grained dynamics of a model for two groups of *heterogeneous* leaders (with no followers) shown in Eq. (5), and compare the results of the two different scales. One notable difference from the Kuramoto model is that "oscillators"
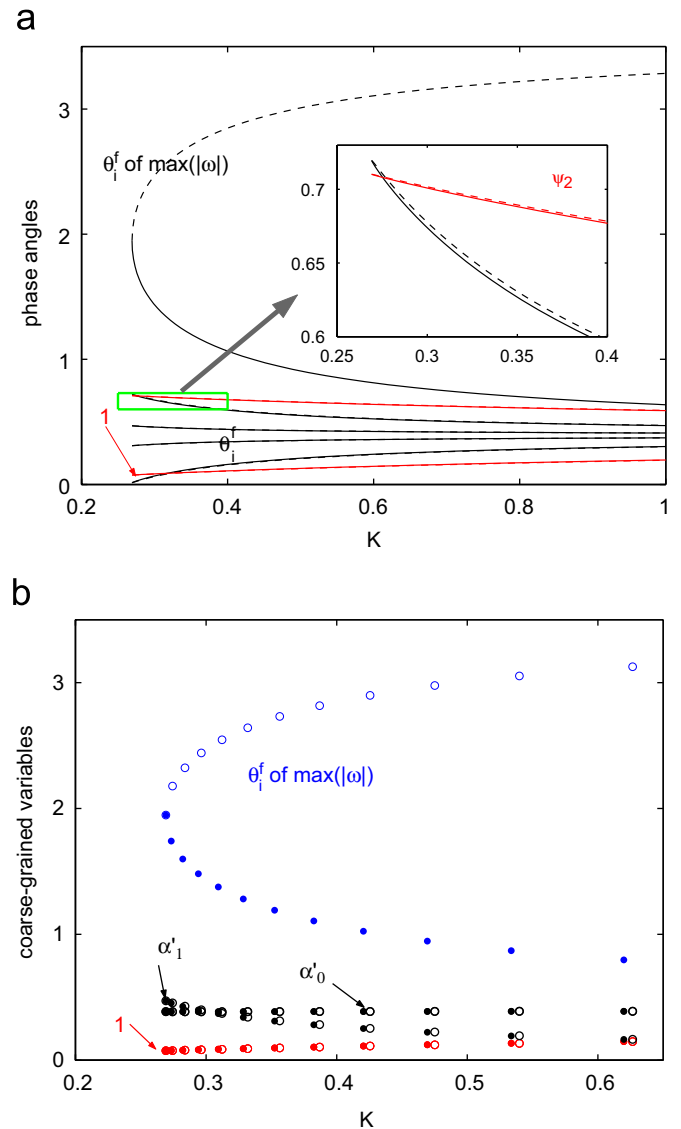
in Eq. (5) do not have finite random variables (natural frequencies), hence there is no onset of the synchronization that occurs at a finite value of K (or, they can be alternatively seen as Kuramoto-like oscillators of zero natural frequencies, which result in the onset at $K = 0$, hence they get synchronized for all K values). The analysis of the minimal model (the first two of Eq. (1) with $N_1 = N_2$, $N_3 = 0$) reveals that for large enough Θ_2 ($> \sim \pi/2$) the system exhibits bistability for a certain

range of K (Nabet et al., 2006), as in the previous case in Section 3. Here, we will vary $\langle \Phi \rangle$ as the main parameter for two different values of K. For large coupling strengths ($K > 2.0$), the bistability in the minimal model appears through a forward pitchfork bifurcation, when Θ_2 is varied as a parameter (Fig. 6). This minimal model can be seen as a special case of the current model, where both $\mathscr{X}$ and Φ are assumed to be delta functions and each group consists of identical individuals.

We begin by asking whether our model for heterogeneous groups exhibits similar types of dynamical behavior. One can also do accelerated computations of steady states using the coarse projective integration, but here we skip such computations and present only the coarse bifurcation analysis results. *Coarse* bifurcation diagrams obtained through the coarse Newton–GMRES method (Kelley, 1995) and pseudo-arc-length continuation (Keller, 1987) (for Gaussian distributions of $\mathscr{X}$ and Φ; $\sigma_{\mathscr{X}} = \sigma_{\Phi} = 0.1$, $N_1 = N_2 = 100$) show that the heterogeneous groups indeed exhibit the same qualitative type of coarse dynamical behavior around the pitchfork bifurcation point (Fig. 7). As we consider symmetric unimodal distribution functions, all the even order chaos coefficients (except for α_0 and β_0) virtually vanish. The diagram for α_0 of the first group $\langle \chi \rangle$ (average direction) exhibits reasonably good quantitative agreement with the corresponding diagram for the minimal model, within fluctuations of finite-size random variables, shown in Figs. 6 and 8. It is interesting to note that at the critical point, all the followers are headed for the same direction ($\alpha_1 = 0$, which corresponds to the "slope" between $\mathscr{X}$ and χ; see Fig. 7(b).

Fig. 7. Coarse-grained bifurcation diagrams observed on the first two chaos coefficients: (a) α_0: the average direction of the first group of leaders and (b) α_1: the "slope" between χ and $\mathscr{X}$, as functions of $\langle \Phi \rangle$. These are blowups of the region around the forward pitchfork bifurcation point in Fig. 6.

The Hermite polynomial expansion converges so quickly that the expansions can be accurate even when truncated at the third order. Due to the reflection symmetry (about $\langle \Phi \rangle / 2$), $\boldsymbol{\beta}$ coefficients have similar structures as the $\boldsymbol{\alpha}$ ones, after proper reflection and translation. Only results on $\boldsymbol{\alpha}$ are presented here. As the coupling strength decreases across $K = 2.0$, the nature of the bifurcation changes (from a pitchfork) to a saddle-node bifurcation (Fig. 8) at $K = 2.0$, which also occurs in the model for homogeneous populations; the nature of the transition between these different bifurcations, a higher codimension bifurcation, has been discussed in Nabet et al. (2006).

4.2. Statistically different groups

So far we have considered statistically similar groups, namely $N_1 = N_2$ and $\sigma_{\mathscr{X}} = \sigma_{\Phi}$; they differed only by
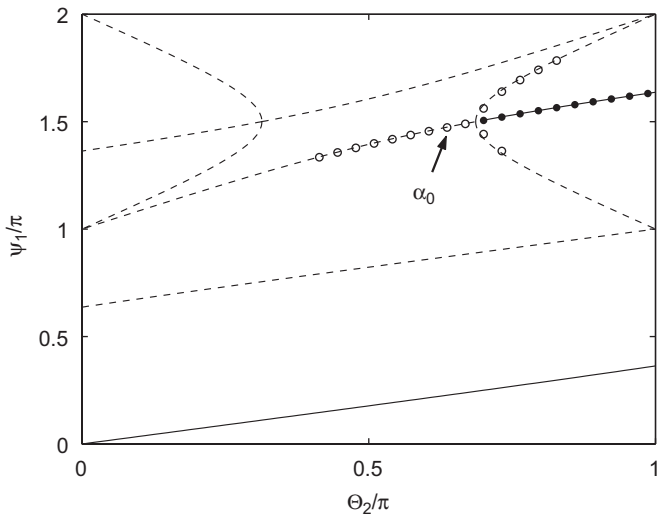
Fig. 6. Lines: a bifurcation diagram observed on ψ_1 in the minimal model (the first two ODEs in Eq. (1) with $N_1 = N_2 = 1$, $N_3 = 0$), for varying Θ_2 at a fixed value of $K = 2.4$, obtained by AUTO2000. For large enough preferred angles ($\Theta_2/\pi > \sim 0.7$), the system becomes bistable through a forward pitchfork bifurcation. Circles: a coarse bifurcation diagram near the pitchfork bifurcation, observed on α_0, as a function of $\langle \Phi \rangle / \pi$, computed by the coarse Newton–GMRES method. Filled (open) circles represent stable (unstable) steady states.
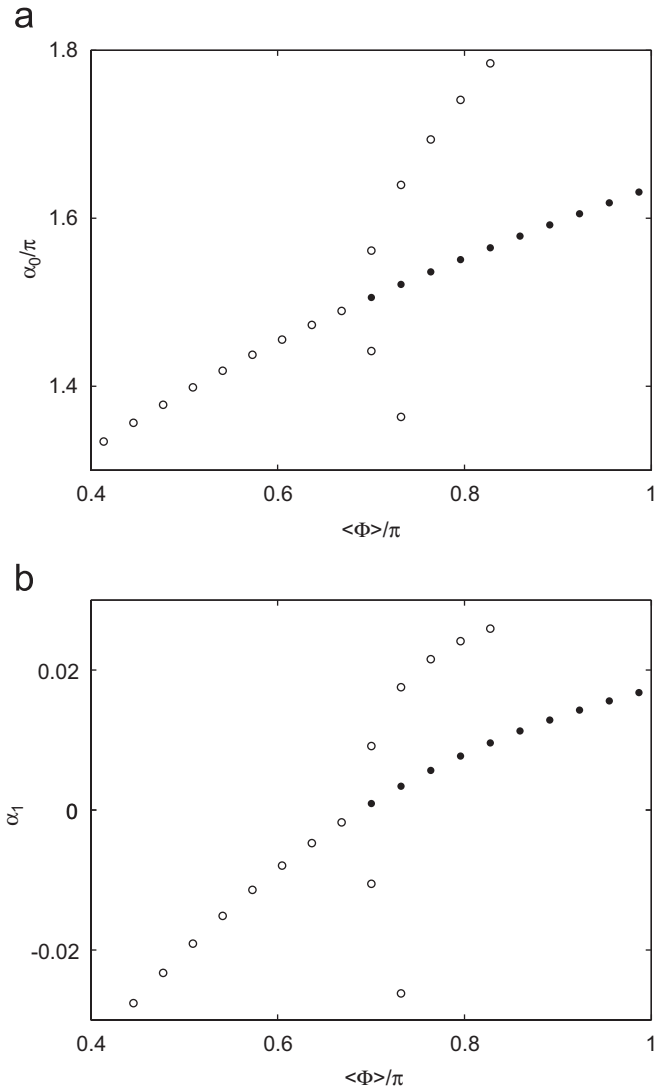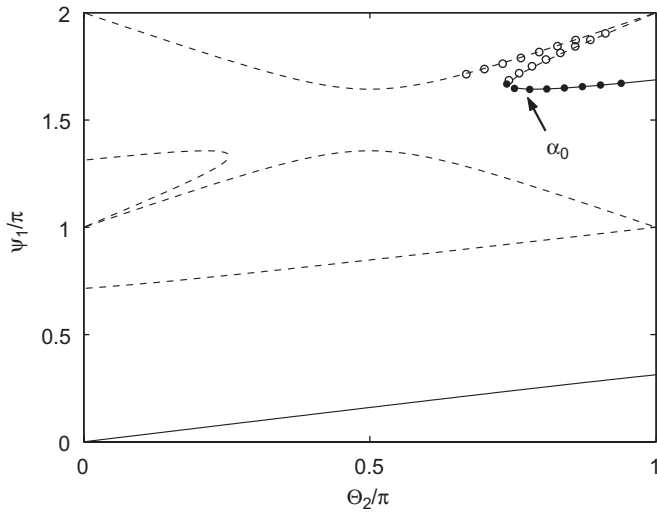
Fig. 8. Lines: a bifurcation diagram for the minimal model of two leaders, for varying Θ_2 at a fixed value of $K = 1.8$, obtained by AUTO2000. For large enough preferred angles ($\Theta_2/\pi > \sim 0.75$), the system becomes bistable, but the nature of the bifurcation is different from that of higher K value cases (a saddle-node vs. a pitchfork bifurcation; see Fig. 6). Circles: a coarse bifurcation diagram observed on the average direction of the first group of leaders (α_0) around the saddle-node bifurcation, as a function of $\langle \Phi \rangle/\pi$, computed via the coarse Newton–GMRES method with continuation. Filled (open) circles represent stable (unstable) steady states.

average preferred directions. It is natural to ask how the dynamics change as the parameters concerned with the distributions (for the preferred directions) are varied. It is readily expected that the essential dynamics of two different size groups can be reflected in the minimal model using two different coupling strengths, which is considered in Nabet et al. (2006). Here, we consider only the cases with varying width of the distributions ($\sigma_\Phi \neq \sigma_\mathscr{X}$), which has no analog in the minimal model.

Coarse bifurcation diagrams for three different Gaussian distributions for $\mathscr{X}$ ($\sigma_\mathscr{X}$ is varied while σ_Φ is kept at 0.1; see Fig. 9) show that the average directions (α_0's) hardly vary with the width of the distributions; the primary parameter that affects on the average direction is the *group size*. For the distributions of different widths, the fixed point computation with continuation fails to converge at different values of α_0's; points marked by arrows in Fig. 9 are the last points the Newton–GMRES computations converged in each case, when approached from the stable branches. Such a failure of convergence can be expected, because the steady states on this unstable branch overlap with another nearby unstable branch (which is not shown in this figure, but was shown in Fig. 8); characterizing the distribution with a few Wiener chaos coefficients does not provide an accurate description any more. The differences between the three cases (of different distribution widths) manifest themselves clearly in higher order chaos coefficients. While the average behavior remains nearly the same (Fig. 9(a)), individuals in the group spread more widely (as reflected in α_1 and higher order coeffi-
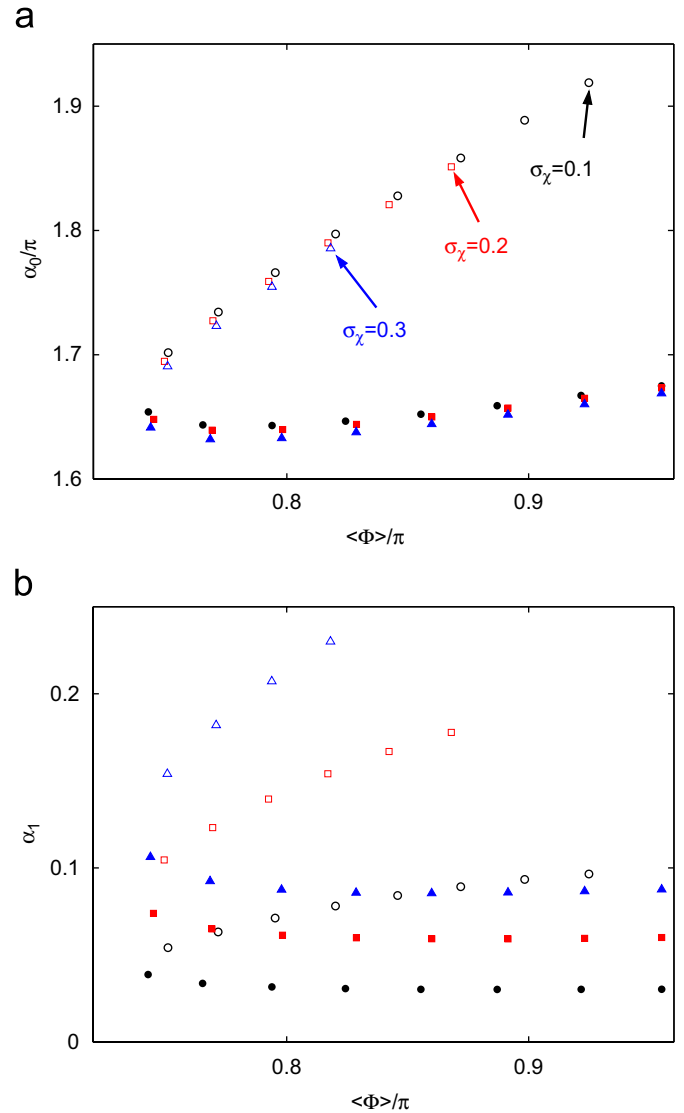

Fig. 9. (Color online) Coarse-grained bifurcation diagrams near a turning point in Fig. 8, for $\mathscr{X}$ distributions of three different widths (the standard deviation $\sigma_\mathscr{X} = 0.1$ for circles; 0.2 for squares; 0.3 for triangles), obtained via the coarse Newton–GMRES method and continuation. The standard deviation for the second group, σ_Φ, is kept the same at 0.1 ($K = 1.8$, $N_1 = N_2 = 100$). Filled and open symbols represent stable and unstable states, respectively. (a) The first chaos coefficients α_0 (average direction of the first group) are nearly the same for the three cases. The difference between the cases becomes apparent in higher order coefficients that reflect the degree of spreading; see α_1 in (b).

cients; Fig. 9(b)), as the width of the random variable (distribution) increases.

5. Conclusions

We have demonstrated a computational venue (an equation-free polynomial chaos approach) to study coarse-grained dynamics of individual-based models accounting for the *heterogeneity* among the individuals in

animal group alignment models. We considered *finite* populations of (I) two "leaders" (which have direct knowledge on preferred directions) and $N(\gg 1)$ uninformed, heterogeneous "followers", and (II) two groups of heterogeneous "leaders". We explored the *coarse-grained*, group level (low-dimensional) dynamics using the polynomial chaos expansion coefficients as coarse-grained observables; these observables account for rapidly developing correlations between random variables, and sufficiently specify both fine-scale and coarse-grained (group-level) dynamical states.

All the analysis in our study was done expressively avoiding the derivation of coarse-grained governing equations, following a *nonintrusive*, equation-free computational approach wrapped around the direct system simulator. It should be noted that we have not assumed that N is infinitely large (so-called the "continuum limit"). Our approach can be used for systems of any finite, large number of populations, and it can be equally applied to various types of random variables (following generalized polynomial chaos) and/or various heterogeneity. We compared our results with those of minimal models that do not account for heterogeneity among the individuals. They show good agreement in the lowest order (i.e., average directions), which clearly highlights the correspondence between the individual- and group-level dynamics (Figs. 6 and 8). Indeed this implies that the results in Nabet et al. (2006), where no heterogeneity is explicitly accounted for, are more robust than demonstrated in that paper alone.

In order to analyze different coarse-grained bifurcations, it became necessary to use different sets of coarse-grained variables, even if the model is *the same* in the fine-scale level (Fig. 5). This clearly shows that an appropriate choice of coarse-grained observables (in terms of which one can obtain useful closures) is an essential step; different coarse-grained observables are required, as the same fine-scale model closes differently.

In the present study, we assumed that the orientational dynamics can be separated from their translational counterpart, and considered the simplest nontrivial cases of all-to-all ("all-visible"), sinusoidal coupling. Our future work will involve the incorporation of the translational dynamics and more complicated coupling/network topology, including heterogeneous couplings. Our work presented here is the first step of our effort toward the development of more detailed (and biologically more plausible) models and their *coarse graining*.

Acknowledgments

References

Acebrón, J.A., Bonilla, L.L., Pérez Vicente, C.J., Ritort, F., Spigler, R., 2005. The Kuramoto model: a simple paradigm for synchronization phenomena. Rev. Mod. Phys. 77, 137–185.

Aoki, I., 1982. A simulation study on the schooling mechanism in fish. Bull. Jap. Soc. Sci. Fish 48, 1081–1088.

Atz, J.W., 1953. Orientation in schooling fishes. In: Proceedings of a Conference on Orientation in Animals. Office of Naval Research, Department of the Navy, Washington, DC, pp. 103–130 (Section 2).

Ben-Jacob, E., Cohen, I., Levine, H., 2000. Cooperative self-organization of microorganisms. Adv. Phys. 49, 395–554.

Camazine, S., Deneubourg, J.-L., Franks, N.R., Sneyd, J., Theraulaz, G., Bonabeau, E. (Eds.), 2001. Self-Organization in Biological Systems. Princeton University Press, Princeton and Oxford.

Couzin, I.D., Krause, J., James, R., Ruxton, G.D., Franks, N.R., 2002. Collective memory and spatial sorting in animal groups. J. Theor. Biol. 218, 1–11.

Couzin, I.D., Krause, J., Franks, N.R., Levin, S.A., 2005. Effective leadership and decision-making in animal groups on the move. Nature 433, 513–516.

Czirók, A., Vicsek, T., 2001. Collective motion. In: Viscek, T. (Ed.), Fluctuations and Scaling in Biology. Oxford University Press, Oxford, pp. 177–242.

Deneubourg, J.L., Goss, S., 1989. Collective patterns and decision making. Ethol. Ecol. Evol. 1, 295–311.

Doedel, E.J., et al., 2000. A numerical bifurcation analysis software freely. Available from ⟨http://indy.cs.concordia.ca/auto/⟩.

Flierl, G., Grünbaum, D., Levin, S., Olson, D., 1999. From individuals to aggregations: the interplay between behavior and physics. J. Theor. Biol. 196, 397–454.

Gear, C.W., Kevrekidis, I.G., 2003. Projective methods for stiff differential equations: problems with gaps in their eigenvalue spectrum. SIAM J. Sci. Comput. 24 (4), 1091–1106.

Ghanem, R., 1999. Ingredients for a general purpose stochastic finite elements formulation. Comput. Methods Appl. Mech. Eng. 168, 19–34.

Ghanem, R., Spanos, P., 1991. Stochastic Finite Elements: A Spectral Approach. Springer, New York.

Hunter, J.R., 1966. Procedure for analysis of schooling behavior. J. Fish. Res. Board Canada 23 (4), 547–562.

Jadbabaie, A., Lin, J., Stephen Morse, A., 2003. Coordination of groups of mobile autonomous agents using nearest neighbor rules. IEEE Trans. Automat. Control 48, 988–1000.

Jardak, M., Su, C.-H., Karniadakis, G.E., 2002. Spectral polynomial chaos solutions of the stochastic advection equation. J. Sci. Comput. 17, 319–338.

Keller, H.B., 1987. Lectures on Numerical Methods in Bifurcation Theory. Tata Institute of Fundamental Research, Lectures on Mathematics and Physics. Springer, New York.

Kelley, C.T., 1995. Iterative Methods for Linear and Nonlinear Equations, Frontiers in Applied Mathematics, vol. 16. SIAM, Philadelphia.

Kevrekidis, I.G., Gear, C.W., Hyman, J.M., Kevrekidis, P.G., Runborg, O., Theodoropoulos, C., 2003. Equation-free coarse-grained multiscale computation: enabling microscopic simulators to perform system-level tasks. Commun. Math. Sci. 1 (4), 715–762 e-print physics/0209043.

Kevrekidis, I.G., Gear, C.W., Hummer, G., 2004. Equation-free: the computer-assisted analysis of complex, multiscale systems. AIChE J. 50, 1346–1355.

Kosterlitz, J.M., Thouless, D.J., 1973. Ordering, metastability and phase transitions in two-dimensional systems. J. Phys. C Solid State Phys. 6, 1181–1203.

Kuramoto, Y., 1984. Chemical Oscillations, Waves, and Turbulence. Springer, New York.

Leonard, N.E., Paley, D., Lekien, R., Sepulchre, R., Fratantoni, D.M., Davis, R., 2007. Collective motion, sensor networks and ocean

sampling. Proceedings of the IEEE, Special Issue on The Emerging Technology of Networked Control Systems, to appear.

Lucor, D., Xiu, D., Karniadakis, G., 2001. Spectral representations of uncertainty in simulations: algorithms and applications. In: Proceedings of the International Conference on Spectral and High Order Methods (ICOSAHOM-01), Uppsala, Sweden.

Mikhailov, A.S., Zanette, D., 1999. Noise-induced breakdown of collective coherent motion in swarms. Phys. Rev. E 60, 4571–4575.

Moon, S.J., Ghanem, R., Kevrekidis, I.G., 2006. Coarse-graining the dynamics of coupled oscillators. Phys. Rev. Lett. 96, 144101.

Nabet, B., Leonard, N.E., Couzin, I.D., Levin, S.A., 2006. Leadership in animal group motion: a bifurcation analysis. In: Proceedings of the 17th International Symposium on Mathematical Theory of Networks and Systems, Kyoto, Japan, July 2006.

Parrish, J.K., Viscido, S.V., Grünbaum, D., 2002. Self-organized fish schools: an examination of emergent properties. Biol. Bull. 202, 296–305.

Partridge, B.L., 1982. The structure and function of fish schools. Sci. Am. 246, 90–99.

Partridge, B.L., Pitcher, T.J., 1979. Evidence against a hydrodynamic function for fish schools. Nature 279, 418–419.

Partridge, B.L., Pitcher, T.J., 1980. The sensory basis of fish schools: relative role of lateral line and vision. J. Comp. Physiol. 135, 315–325.

Pitcher, T.J., Partridge, B.L., Wardle, C.S., 1976. A blind fish can school. Science 194, 963–965.

Reynolds, C., 1987. Flocks, birds, and schools: a distributed behavioral model. Comput. Graph. 21 (4), 25–34.

Rico-Martinez, R., Gear, C.W., Kevrekidis, I.G., 2004. Coarse projective kMC integration: forward/reverse initial and boundary value problems. J. Comp. Phys. 196, 474–489.

Sepulchre, R., Paley, D., Leonard, N.E., 2005. Collective motion and oscillator synchronization. In: Kumar, V., Leonard, N., Morse, A.S. (Eds.), Cooperative Control: A Post-Workshop Volume, 2003 Block Island Workshop on Cooperative Control. Springer, Berlin.

Theodoropoulos, C., Qian, Y.H., Kevrekidis, I.G., 2000. "Coarse" stability and bifurcation analysis using time-steppers: a reaction–diffusion example. Proc. Natl Acad. Sci. USA 97, 9840–9843.

Toner, J., Tu, Y., 1995. Long-range order in a two-dimensional dynamical XY model: how birds fly together. Phys. Rev. Lett. 75, 4326–4329.

Toner, J., Tu, Y., 1998. Flocks, herds, and schools: a quantitative theory of flocking. Phys. Rev. E 58, 4828–4858.

Topaz, C.M., Bertozzi, A.L., Lewis, M.A., 2006. A nonlocal continuum model for biological aggregation. Bull. Math. Biol. 68, 1601–1623.

van Olst, J.C., Hunter, J.R., 1970. Some aspects of the organization of fish schools. J. Fish. Res. Board Canada 27, 1225–1238.

Vicsek, T., Czirók, A., Ben-Jacob, E., Cohen, I., Shochet, O., 1995. Novel type of phase transition in a system of self-driven particles. Phys. Rev. Lett. 75, 1226–1229.

Weidlich, W., 1991. Physics and social science—the approach of synergetics. Phys. Rep. 204, 1–163.

Wiener, N., 1938. The homogeneous chaos. Am J. Math. 60, 897–936.

Wilson, E.O., 1975. Sociobiology: The New Synthesis. Harvard University Press, Cambridge.

Xiu, D., Karniadakis, G.Em., 2002. The Wiener–Askey polynomial chaos for stochastic differential equations. SIAM J. Sci. Comput. 24, 619–644.

Xiu, D., Kevrekidis, I.G., Ghanem, R., 2005. An equation-free, multiscale approach to uncertainty quantification. Comput. Sci. Eng. 7, 16–23.